Microchim Acta (2017) 184:781–790
DOI 10.1007/s00604-016-2015-0

ORIGINAL PAPER

Titanium dioxide anchored graphene oxide nanosheets for highly selective voltammetric sensing of dopamine

Durairaj Santhakumar Ruby Josephine[1] · **Kaliyamoorthy Justice Babu**[2] · **George peter Gnana kumar**[2] · **Kunjithapatham Sethuraman**[1]

Received: 30 April 2016 / Accepted: 7 November 2016 / Published online: 4 January 2017

Abstract The authors report on an efficient method for the voltammetric sensing of dopamine (DA) by using an electrode modified with alternating monolayers of graphene oxide (GO) and Titanium dioxide (TiO_2) nanoparticles anchored GO nanosheets (NSs)). The as-prepared nanostructures were characterized by photoluminescence spectroscopy, powder X-ray diffraction, Raman spectroscopy, FT-IR spectroscopy, transmission electron microscopy, scanning electron microscopy, atomic force microscopy and Energy Dispersive X-ray Analysis (EDAX) techniques. The GO/TiO_2 nanocomposite (NC) was deposited on a glassy carbon electrode (GCE), where it displayed an excellent electrocatalytic activity toward the oxidation of DA, owing to its excellent conductivity, high specific surface area, enhanced interfacial contact and more negative zeta potential. Figures of merit include (a) a fast response (5 s), (b) a wide linear range (between 0.2 and 10 μM of DA) (c) a particularly low detection limit (27 nM), (d) a working potential as low as 0.25 V (vs. Ag/AgCl) and (e) a sensitivity of 1.549 μA·$\mu M^{-1}\cdot cm^{-2}$. The GO/TiO_2/GCE exhibited excellent selectivity over the other interferences as revealed by the differential pulse voltammetric and amperometric studies. The analysis of spiked urine samples resulted in recoveries in the range of 96 to 106%, with RSDs between 3.8 and 5.2%.

Keywords Monolayer · Photoluminescence · X-ray diffraction · FT-IR · Transmission electron microscopy · Scanning electron microscopy · Atomic force microscopy · EDAX · Zeta potential · Differential pulse voltammetry · Urine analysis

Introduction

Dopamine (DA) is an electroactive catecholamine neurotransmitter present in the extracellular fluid of the brain for the proper neurological functions including emotion, movement, attention, learning and memory [1, 2]. A low DA level causes neurological disorder of Parkinson's disease. The high exposure of DA can lead to abnormally high pressure, pleasurable feelings and euphoria, which urges the development of sensitive, selective, economical and efficient DA sensors [2]. Currently several conventional methods are available for the detection of DA including chromatography, fluorimetry, capillary electrophoresis and mass spectrometry [3]. However, the aforementioned techniques exhibited certain hindrances including time consumption, laborious, difficult work up and requirement of large quantity of analyte [3, 4]. Owing to the superior properties such as cost effectiveness, simplicity, feeble requirement of analyte, high accuracy and fast response, electrochemical technique has grabbed its intensive applications in DA detection [4]. However, the prime difficulty of electrochemical DA sensors is the overlapping oxidation potential of uric acid (UA) and ascorbic acid (AA) and its fouling effects at electrode surface, which collectively limited its sensitivity and selectivity [4, 5]. Also the development of DA sensor for the precise and selective measurement of DA at

Electronic supplementary material The online version of this article (doi:10.1007/s00604-016-2015-0) contains supplementary material, which is available to authorized users.

✉ George peter Gnana kumar
kumarg2006@gmail.com

✉ Kunjithapatham Sethuraman
sethuraman_33@yahoo.com

[1] School of Physics, Madurai Kamaraj University, Madurai, Tamil Nadu -625021, India

[2] Department of Physical Chemistry, School of Chemistry, Madurai Kamaraj University, Madurai, Tamil Nadu -625021, India

the low level characteristic of living system (26–40 $nmolL^{-1}$) is still under crisis [4–7]. Hence, it is clear that, the modification of a simple, low cost, ease of processing and environmentally benign catalytic material is highly essential.

On the basis of above, number of research efforts has been achieved on the precious metals and its alloy nanoparticles (NPs) for the detection of DA. However, the precious metal NPs usually suffer from scarcity, aggregation and surface poisoning issues. To overcome these obstacles, numerous research efforts have been achieved with non-precious metals, metal oxides and semiconductors including iron oxide (Fe_3O_4), manganese dioxide (MnO_2) and titania (TiO_2) based nanostructures [4–6]. Among the aforementioned nanostructures, TiO_2 has been considered as a highly potent electroactive material, owing to its unique photovoltaic, photoconductive and catalytic properties. Furthermore, the low cost, non-toxicity, simple preparation and biocompatibility of TiO_2 nanomaterials increased it's competence further. However, TiO_2 nanomaterials still intricate with the modest electrical conductivity, inferior mechanical stability, low surface area, and limited electrocatalytic activity [8]. The aforementioned limitations could be effectively overwhelmed by anchoring the nanostructures over the active carbon support. Among the active carbon materials studied, graphene is considered as an excellent support, owing to its large aspect ratio, high electrical conductivity, stability and superior mechanical and optical properties [9–14]. In specific, graphene oxide (GO) is even more superior and versatile in comparison with graphene in terms of its interaction with the its functional materials, owing to the presence of abundant oxygen labile functional groups [15]. Also the negatively GO sheets can accelerate the interaction with the positively charged DA, which enables the discrimination effects toward AA and UA [16]. Recently, GO based composites have been explored in number of applications including sensor [16], catalysis [17, 18], transparent conducting films [19], paper-like composite materials [20], energy- related materials [21] and in biological and medical applications [22]. In addition, GO has also been employed as an effectual sensor probe toward the quantification of DNA [23], glucose [24], DA [25], etc. On the basis of above, we employed monolayer GO and functionalized monolayer GO as DA sensor.

Owing to its good biocompatibility, high conductivity, elevated surface area, long term chemical stability and more negative zeta potential, TiO_2 has been widely used in the fabrication of electrochemical biosensors [26, 27]. Although few reports have been filed for the quantification of DA by using GO/TiO_2 composite, the obtained results are not compatible for the practical applications. Hence, this report is aimed to provide the highly sensitive and selective electrochemical DA sensors by using the as-prepared GO/TiO_2 composite.

Experimental

Materials and characterizations

Graphite powder is purchased from sigma aldrich (www.sigmaaldrich.com), whereas potassium permanganate ($KMnO_4$, 99%), sulfuric acid (H_2SO_4, 98%), de-ionized water (DI), hydrogen peroxide (H_2O_2, 30% purified), hydrochloric acid (HCL, 37%), titanium di oxide (TiO_2) were purchased from alfa aesar (www.alfa.com). All the raw materials were of analytical grade and used further. Further the dopamine (DA) and other analysts such as ascorbic acid (AA), uric acid (UA), urea (U), glucose (Glc) and, L-dopa (LD), phenethylamine (PEA) and sodium chloride (NaCl) were purchased from sigma aldrich (www.sigmaaldrich.com). Potassium permanganate ($KMnO_4$, 99%), sulfuric acid (H_2SO_4, 98%), hydrogen peroxide (H_2O_2, 30% purified), hydrochloric acid (HCL, 37%), TiO_2 were purchased from Alfa Aesar (www.alfa.com). Graphite powder, DA, AA, UA, urea (U), glucose (Glu) and, L-dopa (LD), phenethylamine (PEA) and sodium chloride (NaCl) were purchased from sigma Aldrich (www.sigmaaldrich.com).

The as-prepared nanomaterials were characterized by using atomic force microscopy (AFM) (non-contact mode, A100 SGS, APE Research) (http://www.aperesearch.com), scanning electron microscopy (SEM) with EDAX analysis (JEOL (JSM- 5610LV) (http://www.jeolusa.com), high-resolution transmission electron microscopy (HRTEM) (TECNAI, model - CM 200), powder x-ray diffraction (XRD) (Brucker D8 Advance XRay Diffractometer) (https://www.bruker.com), Raman (LabRam HR800 micro-Raman) (https://www.horiba.com), FT-IR (Brukeroptik) (https://www.bruker.com) and Shimadzu-UV 2450 double beam spectrophotometer (https://www.ssi.shimadzu.com), and RF-5301 spectroflurometer (https://www.ssi.shimadzu.com) in the wavelength range of 300–800 nm respectively. Furthermore, the electrochemical studies of the samples are analyzed via CHI650D electrochemical analyzer (CH Instruments, Austin, TX, USA) (https://www.chinstruments.com) in a three electrode system such as GCE (glassy carbon electrode) as working electrode ($0.07cm^2$), Pt wire as counter electrode, Ag/AgCl (1 M - KCl) as reference electrode with a 0.1 M phosphate buffer electrolyte of pH 7.2 in the presence of analyst DA.

Synthesis of graphene oxide nanosheets and graphene oxide/titanium dioxide nanocomposite

GO NSs were synthesized according to Hummers and Offeman's [28, 29] method followed by exfoliation. An appropriate amount of GO suspension was concurrently mixed with 10 wt% of TiO_2 NPs suspended in 200 mL of DI water through sonication for 10 min and the mixed up suspension was magnetically stirred for 24 h. The above mixture was then washed with DI water through centrifugation at 5000 rpm for 15 min and the precipitate was collected and dried [30].

Modification of electrodes

GCE (diameter of 3 mm and area 0.07 cm^2) was polished sequentially with 1.0, 0.3 and 0.05 mm sized alumina powder and sonicated in DI water, after each stage of polishing. The prepared nanostructures were dispersed in DMF (5 mg mL^{-1}) and 6 μL of the above suspension was dropped on the surface of a polished GCE and dried in air. Further 6 μL of 0.5% Nafion was dropped on the electrode surface and fixed with the catalyst followed by drying at room temperature. GO and GO/TiO_2 nanocatalysts modified GCE are represented as GO/GCE and GO/TiO_2/GCE respectively.

Electrochemical measurements

A conventional three-electrode electrochemical cell assembly involving bare/modified GCEs as a working electrode, a Ag/AgCl as reference electrode and a Pt wire as counter electrode were used to perform the electrochemical experiment. The cyclic voltammetry was performed at a scan rate of 20 mVs^{-1} in 0.1 M phosphate buffer (pH 7.2) under the absence and presence of 50 μM DA. The amperometric experiments were carried out in 0.1 M phosphate buffer with the successive addition of different concentrations of DA at an applied potential of 0.25 V vs. Ag/AgCl. DPV measurements were carried out at bare GCE and GO/TiO_2/GCE in phosphate buffer containing 20 μM DA, 2 mM AA and 0.2 mM UA.

Results and discussion

Choice of materials

To overcome the significant problems of overlapping voltammetric responses of interferences in electrochemical DA sensors, various precious metal nanoparticles including Au, Ag, Pt, Pd and Ru and their alloys were employed, owing to their extraordinary physicochemical properties [1]. However, the surface poisoning and fouling effects exhibited by the precious metal nanoparticles directed the research dimensions toward the environmentally benign and negatively charged TiO_2 nanomaterials. To further enhance the electrochemical quantification of TA, the composite formation of TiO_2 with active GO sheets was achieved.

Morphological and structural studies

AFM topographs of GO and GO/TiO_2 NC and the line profile of GO/TiO_2 NC are depicted in Fig. 1a, b and c respectively. All the recorded morphologies depicted the existence of sheet like features of GO and its NC. The thickness of GO sheets was found to be 1 nm and it is also confirmed that the sheets were well exfoliated down to monolayer sheet of GO (Fig. 1a). Typically, a monolayer GO NSs with oxygen containing functional groups on both sides of the basal plane and edges are in the range of 1–1.3 nm [31]. Figure 1b confirms the presence of TiO_2 NPs as bright dots onto GO NSs of GO/TiO_2 NC. The line profile of GO/TiO_2 NC (Fig. 1c) suggested that 5–10 nm mean diameter sized TiO_2 NPs were embossed on monolayer of GO NSs and the root mean square (RMS) roughness value of GO and GO/TiO_2 NC was found to be 0.256 nm and 2.59 nm, respectively. As evidenced from Fig. 1d, GO NSs appeared to be spread over few micrometers in size, specifying the high aspect ratio. From Fig. 1e, it is clear that TiO_2 were uniformly distributed on the basal planes of GO sheets. The TiO_2 coverage on the surface of GO sheets specified that the strong interaction was exerted between the carbon network of GO and TiO_2 NPs.

XRD measurements were carried out to explore the structural information of GO and GO/TiO_2 NC. GO NSs exhibited an intense diffraction peak at 10.44°, corresponding to the (001) reflection plane with the basal spacing of 0.846 nm, specifying that that the oxygen containing functional groups were intercalated onto the GO layers (Fig. 2 (i) a). The diffraction pattern of GO/TiO_2 exhibited the characteristic diffraction pattern of GO along with the few additional peaks at 25 and 45°, corresponding to (101) and (200) planes, respectively, of the anatase phased TiO_2 NPs (Fig. 2 (i) b). The FT-IR spectrum of GO exhibited the band at 3395 cm^{-1}, which is assigned to the stretching modes of –OH bonds. The band at 1726 cm^{-1} is assigned to stretching vibrations of C = O and peak at 1620 cm^{-1} is consigned to the vibrations of unoxidized graphitic domains, 1225 cm^{-1} is assigned to the stretching vibrations of C-OH and band at 1040 cm^{-1} is assigned to stretching vibration of C-O, which provides evidence for the presence of different types of oxygen containing functional groups including –COOH, −C = O, −C-OH and epoxy group on the GO materials (Fig. 2 (ii) a). The FTIR spectrum of GO/TiO_2 NC is shown in Fig. 2 (ii) b. The

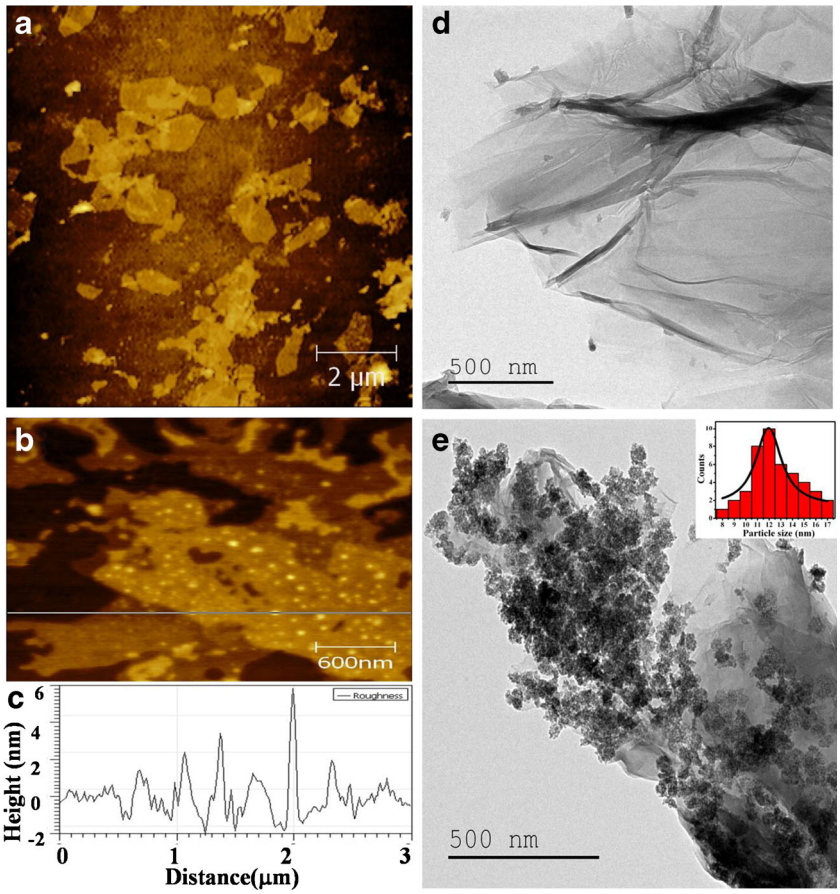

Fig. 1 AFM images of **a** GO and **b** GO/TiO_2 nanostructures and **c** the base plan of GO/TiO_2 nanocomposite and TEM images of **d** GO and e GO/TiO_2 nanostructures (Inset 1e: TiO_2 nanoparticle size distribution histogram)

significant band observed at 510 cm^{-1} represents the Ti–O–Ti bands confirming the presence of TiO_2 on the composite [32]. The Raman spectra of GO NS and GO/TiO_2 NC are shown in Fig. 2 (iii). The Raman spectrum of GO exhibited the prominent peaks at 1326 and 1598 cm^{-1} corresponding to the 'D' and 'G' bands respectively (Fig. 2, (iii) a). Along with the D and G bands, GO/TiO_2 NC exhibited the charactertsic TiO_2 bands of Eg, B1g, A1g, B1g and Eg modes at 144, 197, 399, 516 and 367 cm^{-1}, respectively., which confirmed the composite formation of TiO2 with GO [33].

Electrochemical characterizations

To elucidate the electron transfer behavior of studied electrodes toward the electrochemical detection of DA, the electrochemical responses of bare GCE, GO/GCE and GO/TiO_2/GCE in buffer (pH 7.2) under the absence and presence of 50 μM DA at 20 mVs^{-1} were obtained by using CV and the obtained voltammograms are provided in Fig. 3a. As the pH value of body fluids is close to 7, pH -7.2 is chosen as optimum value for the detection of DA. Under the absence of DA, the studied electrodes exhibited only the background currents, in which GO/TiO_2/GCE displayed the maximum background current, owing to the large surface area and high electrical conductivity, which facilitated the interfacial contact between GO/TiO_2/GCE and phosphate buffer.

The cyclic voltammograms obtained for bare GCE, GO/GCE and GO/TiO_2/GCE in the presence of 50 μM DA in buffer (pH 7.2) at 20 mVs^{-1} are shown in Fig. 3b. Under the presence of DA, bare GCE, GO/GCE and GO/TiO_2/GCE exhibited the legible redox currents, owing to the electroactive analyte DA. The sluggish electrokinetics was observed at bare GCE as evidenced from the weak redox peak currents, which is attributed to the limited electrical conductivity of GCE [4–7, 34]. The oxidation of DA was increased at GO/GCE as evidenced from the increased oxidation current (Ipa) of 0.560 μA vs. Ag/AgCl. In comparison with bare GCE, GO/GCE exhibited the improved electrooxidation of DA, which is attributed to the

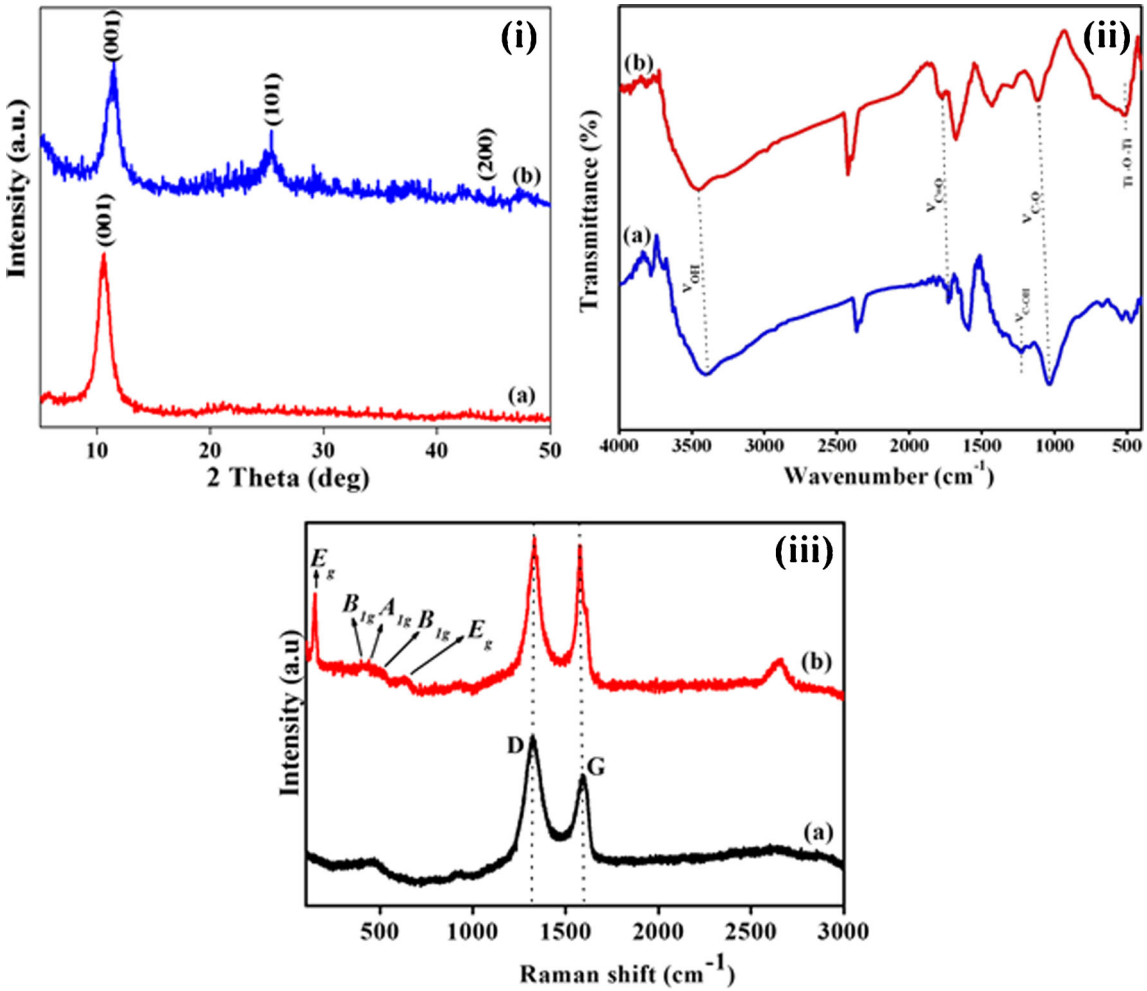

Fig. 2 (*i*) XRD patterns (*ii*) FT-IR spectra and (*iii*) Raman spectra of **a** GO and **b** GO/TiO_2 nanocomposite

elevated surface area and prompt electrical conductivity of GO sheets. The electrostatic interaction exerted between the positively charged DA and negatively charged GO sheets increased electrooxidation of DA. However, the DA oxidation process at GO/GCE is limited, owing to the existence of limited active sites of GO sheets.

The electrooxidation of DA was further enhanced at GO/TiO_2/GCE as observed from the increased Ipa of 0.787 μA vs. Ag/AgCl, which is 1.4 fold higher than that of GO/GCE respectively. Ti^{4+} and O^{2-} chemical states of TiO_2 NPs provided the inbuilt oxygen vacancies that facilitated the number of active sites. It has been reported that TiO_2 exhibited a negative zeta potential and its composite formation with the negatively charged GO provided more negative charge to the corresponding composite, leading to the electrostatic interaction of negatively charged GO/TiO_2 with the positively charged DA. The adsorbed hydroxyl groups on the surface of TiO_2 may induce the strong N-H coordination bond. In addition, the π-conjugation emerged between the aromatic regions of DA and GO of GO/TiO_2 composite facilitated the adsorption of DA over the surface of the resultant composite [22]. The combo of TiO_2 and GO enhanced the electrical conductivity, surface area and charge transport, which promoted the DA accessibility. It has collectively facilitated the interfacial contact between the electrode and electrolyte, and thereby the maximum electrooxidation of DA was promoted. The involved mechanism is put forth as follows: DA was electrochemically oxidized at GO/TiO_2, leading to the formation of dopamine-o-quinone (DOQ) with the liberation of H^+ and e^- in the forward scan. In the reverse scan, DOQ was electrochemically reduced into DA with the aid of liberated H^+ and e^- (Fig. 3c) [4–7, 34].

The electrokinetics involved in DA oxidation at GO/TiO_2/GCE was evaluated in 50 μM DA in buffer (pH 7.2) as a function of scan rate ranging from10

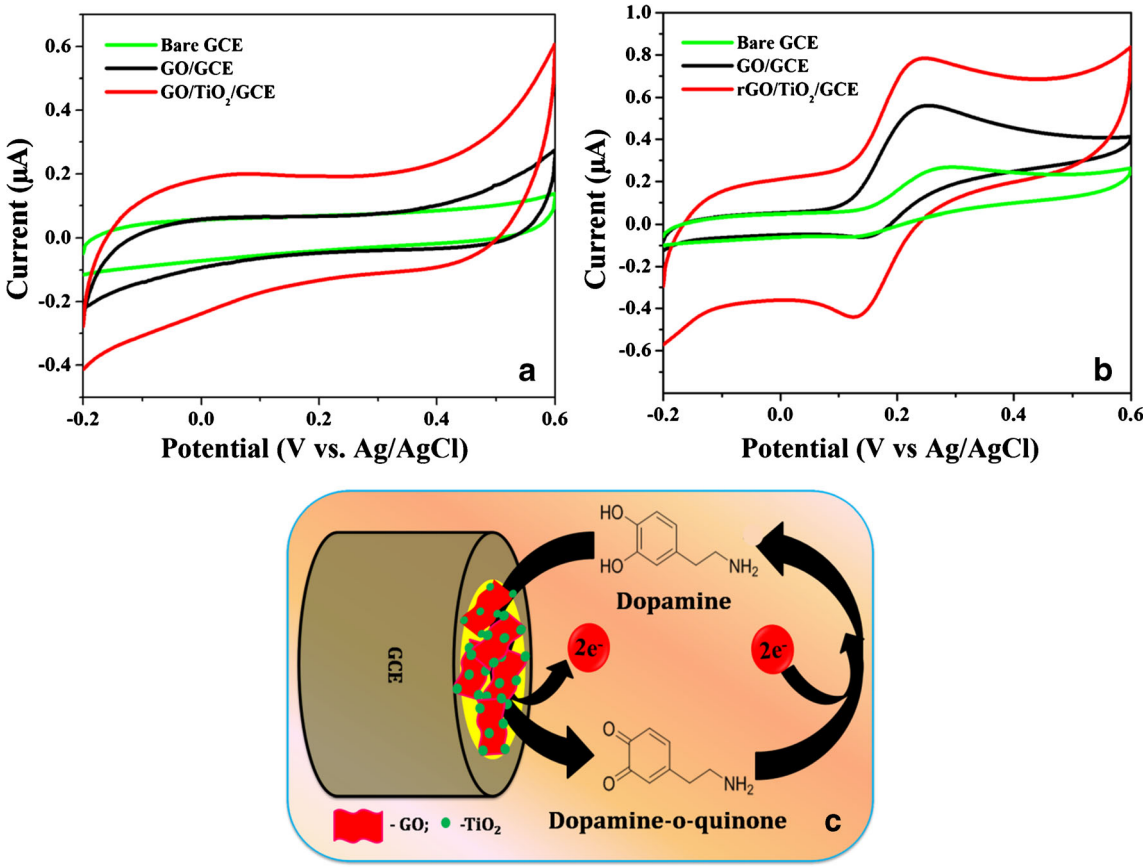

Fig. 3 CVs of studied electrodes under the **a** absence and **b** presence of 50 μM DA in 0.1 M phosphate buffer (pH 7.2) at a scan rate of 20 mVs^{-1} **c** Plausible mechanism for electrocatalytic oxidation of DA at $GO/TiO_2/GCE$

to100 mVs^{-1} (Fig. 4a). From the voltammetric behavior of $GO/TiO_2/GCE$, it is observed that oxidation and reduction peak currents were linearly increased with an increase in scan rate. It is clear that the redox peak currents were linearly scaled with the square root of scan rates ($v^{1/2}$). The fitted regression equations can be expressed as follows: Ipa (μA) = − 0.7791 + 0.3367 v (mVs^{-1}) with a correlation coefficient of (R) = 0.996, n = 10, and Ipc (μA) = 0.6592–0.2446 v (mVs^{-1}) (R = 0.995, n = 10) (Fig. 4 b).

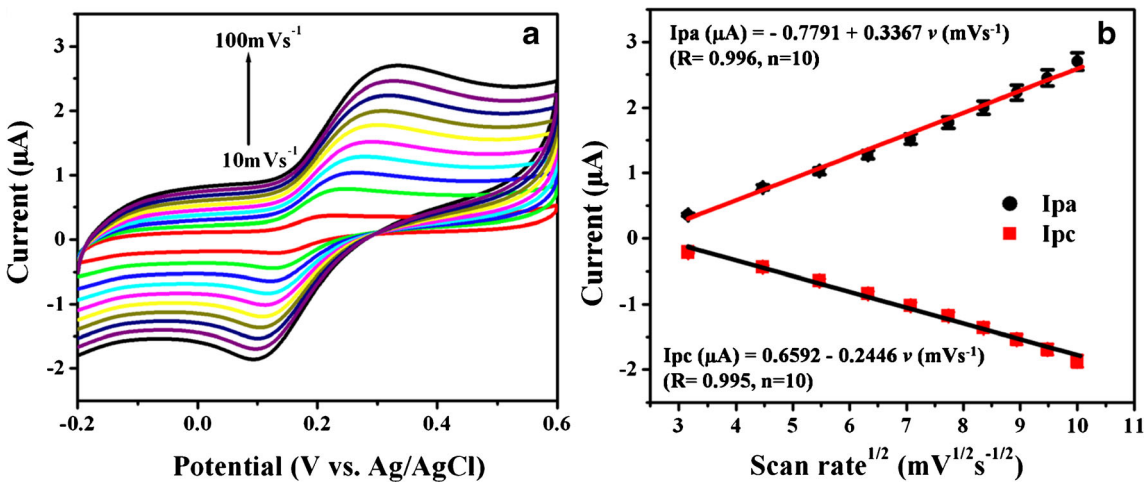

Fig. 4 **a** CVs of $GO/TiO_2/GCE$ in the presence of 50 μM DA buffer (pH 7.2) at different scan rates ranging from 10 to 100 mVs^{-1} and **b** plot of peak current (Ip) vs. square root of scan rates ($v^{1/2}$)

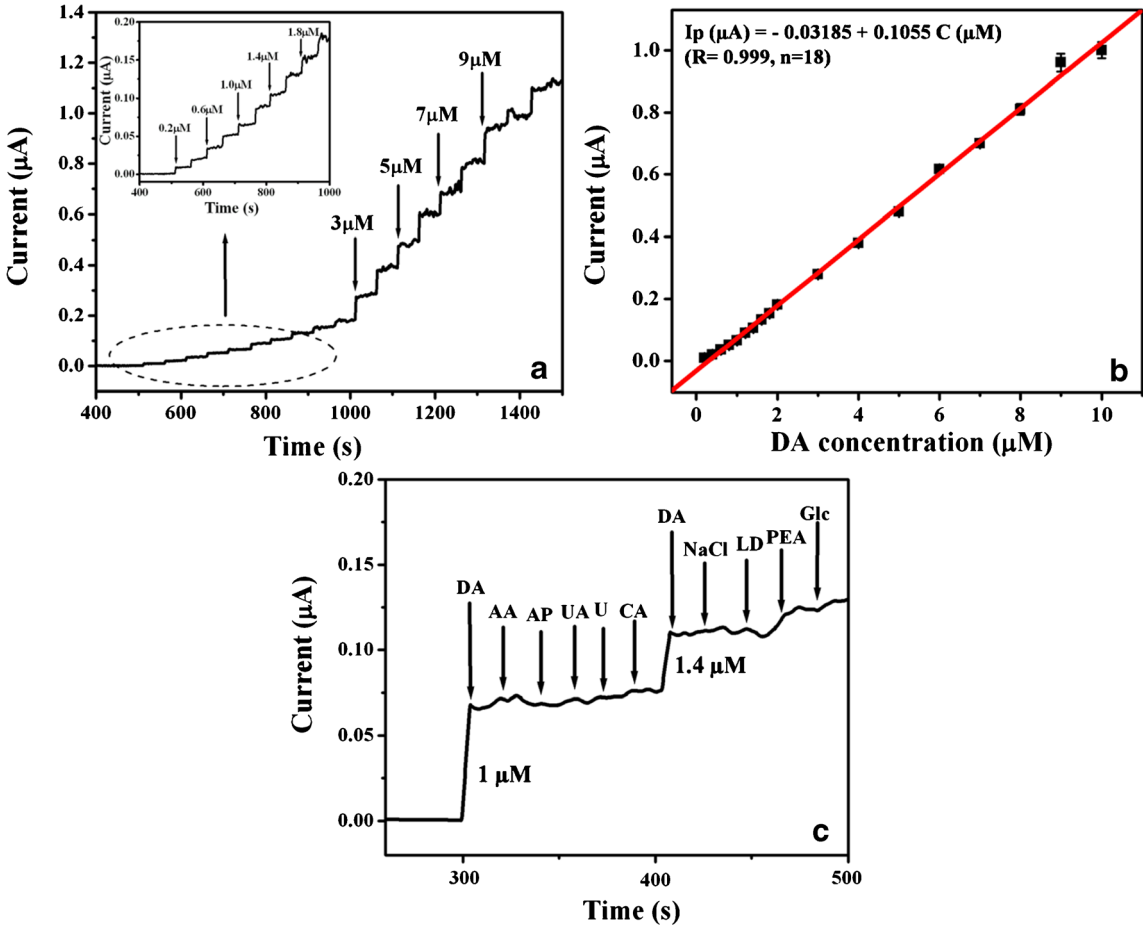

Fig. 5 **a** Amperometry i-t curve of GO/TiO_2/GCE in buffer with successive additions of different concentrations of DA at 0.25 V vs. Ag/AgCl **b** the corresponding calibration curves for current vs. concentration of DA at 0.25 V vs. Ag/AgCl and **c** Interference studies of GO/TiO_2/GCE buffer with the addition of DA and interfering species at 0.25 V vs. Ag/AgCl

Amperometry studies

The amperometric current-time response is a well-established technique for the determination of sensing characteristics of synthesized catalysts. The amperometric response at GO/TiO_2/GCE toward DA was investigated with the successive addition of different concentrations of DA into the continuously stirred buffer at a constant potential of 0.25 V vs. Ag/AgCl and the obtained amperometric responses are given in Fig. 5a. The amperometric response of GO/TiO_2/GCE toward the oxidation of DA was measured as a function of DA concentration and the oxidation peak current was gradually increased with an increase in the DA concentration ranging from 0.2 μM to 10 μM and the fitted regression equation is calculated to be Ip (μA) = − 0.03185 + 0.1055 C (μM) (R = 0.999, n = 18) (Fig. 5b), implying the wide linear range for the fabricated sensor. The fabricated sensor accomplished 95% of the steady state current at 5 s, indicating that GO/TiO_2/GCE displayed very fast amperometric response behavior toward DA. GO/TiO_2/GCE exhibited the low detection limit of 27 nM with the signal to noise ratio of 3 with the wide linear range of 0.2–10 μM and the sensitivity of GO/TiO_2/GCE was measured to be 1.549 μA μM^{-1} cm^{-2}. The fabricated GO/TiO_2/GCE exhibited the excellent catalytic performances toward DA oxidation, owing to the large surface area, high electrical conductivity, high absorptivity, and excellent affinity toward DA. To retard the electron-hole carrier recombination of GO, TiO_2 was decorated over the GO sheets and the charge recombination rate was lowered for GO/TiO_2 NC from that of GO sheets, which pronounced the electrocatalytic activity of GO/TiO_2 composite. The facilitated reactivity of GO/TiO_2 NC is also attributed to the inherent oxygen vacancies, which provided the abundant active sites for the DA

sensing. The obtained electroanalytical performances of GO/TiO_2 sensor were suitably compared in Table S1 (ESM) with the reported literatures and it is clear that the fabricated sensors exhibited lower detection limit and wide linear range toward the DA oxidation than that of previous reports.

Interference studies

To evaluate the selectivity performances of fabricated sensors, the interference studies were achieved at GO/TiO_2/GCE by the successive addition of DA with interfering species such as ascorbic acid (AA), acetaminophen (AP), uric acid (UA), Urea (U), citric acid (CA),Glucose (Glc), sodium chloride (NaCl), L-dopa (LD) and phenethylamine (PEA) buffer (pH 7) solution at an applied potential of 0.25 V vs. Ag/AgCl (Fig. 5c). It is clearly observed that GO/TiO_2/GCE has not exhibited any significant amperometric responses toward the interferences including AA, UA, U, AP, CA and Glc. However, GO/TiO_2/GCE has exhibited an obvious amperometric oxidation current toward DA (1 μM and 1.4 μM) (Fig. 5c).The as-fabricated GO/TiO_2/GCE has not exhibited any obvious current reponse to the amine functionalized LD and PEA, owing to their oxidation potentials of 0.42 and -0.17 V vs. Ag/AgCl, respectively. PEA [35, 36]. The observations suggested that the synthesized GO/TiO_2 demonstrated a good specificity toward the DA detection and the obtained high selectivity is attributed to the electrostatic interaction, N-H coordination and π-conjugation between the DA and GO/TiO_2.

Reproducibility and long-term stability of the dopamine sensor

The reproducibility and operational stability of GO/TiO_2/GCE were evaluated toward DA oxidation through the amperometric response of the electrode in 50 μM DA solution in buffer. The oxidation current response of GO/TiO_2/GCE exhibited a relative standard deviation (RSD) of 3.5%, which displays the good reproducibility of the system. Furthermore, the long-term stability of GO/TiO_2 was investigated through the amperometric response for every 2 days and the fabricated sensor is found to retain 95% of initial response after a month of storage. From the obtained results it is clear that the TiO_2 NPs in GO NSs are retained even after several experiments, ensuring the long-term operational stability of the proposed system.

Real sample analysis

To evaluate the applicability of as-fabricated sensor in clinical field, the detection of DA in human urine sample was evaluated at GO/TiO_2/GCE. Human urine samples were collected from two healthy men. The samples were diluted with buffer (pH 7.2) with the ratio of 1:100 (*v*/v) and the analyzed urine sample was found to be free of DA in the experimental results. The recoveries and relative standard deviation (RSD) of DA for the real sample was assessed at two different spiked concentration levels (5 and 10 μM) under the similar experimental conditions by using the standard addition method and the results are listed in Table 1. The sensor exhibited the recoveries in the range of 96 to 106% with the RSD of 3.8–5.2%. These experimental results obviously confirmed that the recoveries and RSD of the DA sensor in the spiked human urine samples were considerably acceptable and thus proven the practicability of constructed sensor toward real sample analysis.

Conclusions

In summary, TiO_2 nanoparticles were effectively anchored over the GO sheets without any surfactants and the as-prepared composite was well characterized by using number of analytical techniques. The as-prepared NC was effectively exploited as an electrochemical DA sensor probe in neutral conditions. The as-fabricated DA sensor exhibited the excellent electrochemical performances including fast response time, low detection limit, high sensitivity, good stability, reproducibility and high selectivity, that holds great opportunities for the next generation DA sensors in clinical purposes

Table 1 Determination of DA in human urine samples at GO/TiO_2/GCE

Sample used	DA added (μM)	DA found (M)	RSD[a] (%)	Recovery (%)
1	5	4.8	4.8	96
	10	10.4	4.2	104
2	5	5.3	5.2	106
	10	9.8	3.8	98

[a] Relative standard deviation (RSD) of five independent measurements

Acknowledgments The authors acknowledge DST-FIST program of School of Physics, Madurai Kamaraj University for providing XRD facility and DST-PURSE program of School of Physics, Madurai Kamaraj University for providing AFM and UGC-UPE program of Madurai Kamaraj University for HR-TEM facility. This research was supported by University Grants Commission Major project Grant No.: MRP-MAJOR-CHEM-2013-36681. D.S.R. J and K.J. B gratefully acknowledge UGC- New Delhi and Madurai Kamaraj University, Madurai for Non-NET fellowship.

Compliance with ethical standard The author(s) declare that they have no competing interests.

References

1. Yusoff N, Pandikumar A, Ramaraj R, Ngee LH, Huang NM (2015) Gold nanoparticle based optical and electrochemical sensing of dopamine. Microchim Acta 182:2091–2114. doi:10.1007/s0060401516092
2. Sanghavi BJ, Wolfbeis OS, Hirsch T, Swami NS (2015) Nanomaterial based electrochemical sensing of neurological drugs and neurotransmitters. Microchim Acta 182:141. doi:10.1007/s0060401413084
3. Pradhan T, Jung HS, Jang JH, Kim TW, Kang C, Kim JS (2014) Chemical sensing of neurotransmitters. Chem Soc Rev 43:4684–4713. doi:10.1039/C3CS60477B
4. Pandikumar A, How GTS, See TP, Omar FS, Jayabal S, Kamali KZ, Yusoff N, Jamil A, Ramaraj R, John SA, Limbe HN, Huang NM (2014) Graphene and its nanocomposite material based electrochemical sensor platform for dopamine. RSC Adv 4:63296–63323. doi:10.1039/c4ra13777a
5. Salamon J, Sathishkumar Y, Ramachandran K, Lee YS, Yoo DJ, Kim AR, GnanaKumar G (2015) One-pot synthesis of magnetite nanorods/graphene composites and its catalytic activity toward electrochemical detection of dopamine. Biosens Bioelectron 64:269–276. doi:10.1016/j.bios.2014.08.085
6. Rani GJ, Babu KJ, GnanaKumar G, Rajan MAJ (2016) *Watsonia meriana* Flower like Fe_3O_4/reduced graphene oxide nanocomposite for the highly sensitive and selective electrochemical sensing of dopamine. J Alloys Compd 688:500–512. doi:10.1016/j.jallcom.2016.07.101
7. Jackowska K, Krysinski P (2013) New trends in the electrochemical sensing of dopamine. Anal Bioanal Chem 405:3753–3771. doi:10.1007/s00216-012-6578-2
8. LiXia Y, ShengLian L, QingYun CAI, ShouZhuo YAO (2010) A review on TiO_2 nanotube arrays: fabrication, properties, and sensing applications. Chin Sci Bull 55:331–338. doi:10.1007/s11434-009-0712-3
9. Zhou M, Zhai Y, Dong S (2009) Electrochemical sensing and biosensing platform based on chemically reduced graphene oxide. Anal Chem 81:5603–5613. doi:10.1021/ac900136z
10. Zhou TN, Qi XD, Fu Q (2013) The preparation of the poly(vinyl alcohol)/graphene nanocomposites with low percolation threshold and high electrical conductivity by using the large-area reduced graphene oxide sheets. Express Polym Lett 7(9):747–755. doi:10.3144/expresspolymlett.2013.72
11. Neto AHC, Guinea F, Peres NMR, Novoselov KS, Geim AK (2009) The electronic properties of graphene. Rev Mod Phys 81:1–54. doi:10.1103/RevModPhys.81.109
12. Pop E, Varshney V, Roy AK (2012) Thermal properties of graphene: fundamentals and applications. MRS Bull 37:1273–1281. doi:10.1557/mrs.2012.203
13. Berman D, Erdemir A, Sumant AV (2014) Graphene: a new emerging lubricant. Materials Today 17:31–42. doi:10.1016/j.mattod.2013.12.003
14. Falkovsky LA (2010) Optical properties of graphene. J Phys Conf Ser 129(012004):1–7. doi:10.1088/1742-6596/129/1/012004
15. Sharma D, Kanchi S, Myalowenkosi SI, Bisetty K (2016) Insight into the biosensing of graphene oxide: present and future prospects. Arab J Chem 9:238–261. doi:10.1016/j.arabjc.2015.07.015
16. Gao F, Cai X, Wang X, Gao C, Liu S, Gao F, Wang Q (2013) Highly sensitive and selective detection of dopamine in the presence of ascorbic acid at graphene oxide modified electrode. Sensors Actuators B Chem 186:380–387. doi:10.1016/j.snb.2013.06.020
17. Josephine DSR, Sakthivel B, Sethuraman K, Dhakshinamoorthy A (2015) A titanium dioxide/graphene oxide nanocomposites as heterogeneous catalysts for the esterification of benzoic acid with dimethyl carbonate. Chem Plus Chem 80:1472–1477. doi:10.1002/cplu.201500080
18. Josephine DSR, Sakthivel B, Sethuraman K, Dhakshinamoorthy A (2016) A synthesis, characterization and catalytic activity of CdS-graphene oxide nanocomposites. Chemistry Select 1:2332–2340. doi:10.1002/slct.201600384
19. Zheng Q, Li Z, Yang J, Kim JK (2014) Graphene oxide-based transparent conductive films. Prog Mat Sci 64:200–247. doi:10.1016/j.pmatsci.2014.03.004
20. Dikin DA, Stankovich S, Zimney EJ, Piner RD, Dommett GHB, Evmenenko G, Nguyen ST, Ruoff RS (2007) Preparation and characterization of graphene oxide. Nature lett 448:457–460. doi:10.1038/nature06016
21. Lia F, Jianga X, Zhaoa J, Zhang S (2015) Graphene oxide: a promising nanomaterial for energy and environmental applications. Nano Energy 16:488–515. doi:10.1016/j.nanoen.2015.07.014
22. Yang Y, Asiri AM, Tang Z, Du D, Lin Y (2013) Graphene based materials for biomedical applications. Materials Today 16:365–373. doi:10.1016/j.mattod.2013.09.004
23. Lu CH, Yang HH, Zhu CL, Chen X, Chen GN (2009) A graphene platform for sensing biomolecules. Angew Chem Int Ed 48:4785–4787. doi:10.1002/anie.200901479
24. Zhang H, Huang H, Lin Z, Su X (2014) A turn-on fluorescence-sensing technique for glucose determination based on graphene oxide–DNA interaction. Anal Bioanal Chem 406:6925–6932. doi:10.1007/s00216-014-7758-z
25. Ren H, Kulkarni DD, Kodiyath R, Xu W, Choi I, Tsukruk VV (2014) Competitive adsorption of dopamine and rhodamine 6G on the surface of graphene oxide. ACS Appl Mater Interfaces 6:2459–2470. doi:10.1021/am404881p
26. Bai J, Zhou B (2014) Titanium dioxide nanomaterials for sensor applications. Chem Rev 114:10131–10176. doi:10.1021/cr400625j
27. Li F, Gan S, Han D, Niu L (2015) Graphene-based Nanohybrids for advanced electrochemical sensing. Electroanalysis 27:2098–2115. doi:10.1002/elan.201500217
28. Hummers WS, Offeman RE (1958) Preparation of graphitic oxide. J Am Chem Soc 80:1339–1339. doi:10.1021/ja01539a017
29. Lin CH, Yeh WT, Chan CH, Lin CC (2012) Influence of graphene oxide on metal-insulator-semiconductor tunneling diodes. Nanoscale Res Lett 7(343):1–6. doi:10.1186/1556-276X-7-343
30. Hong WG, Kim BH, Lee SM, Yu HY, Yun YJ, Jun Y, Lee JB, Kim HJ (2012) Agent-free synthesis of graphene oxide/transition metal oxide composites and its application for hydrogen storage. Int J Hydrog Energy 37:7594–7599. doi:10.1016/j.ijhydene.2012.02.010
31. Zhao J, Liu L, Li F (2015) Graphene oxide: physics and applications, New York Dordrecht London, Springer Heidelberg.

32. Vasconcelos DCL, Costa VC, Nunes EHM, Sabioni ACS, Gasparon M, Vasconcelos WL (2011) Infrared spectroscopy of Titania Sol-gel coatings on 316 L stainless steel. Mater Sci Appl 2:1375–1382. doi:10.4236/msa.2011.210186
33. Fan Y, Lu HT, Liu JH, Yang CP, Jing QS, Zhang YX, Yang XK, Huang KJ (2011) Hydrothermal preparation and electrochemical sensing properties of TiO_2-graphene nanocomposite. Colloids Surf B 83:78–82. doi:10.1016/j.colsurfb.2010.10.048
34. How GTS, Pandikumar A, Ming HN, Ngee LH (2014) Highly exposed {001} facets of titanium dioxide modified with reduced graphene oxide for dopamine sensing. Sci Rep 4(5044):1–8. doi:10.1038/srep05044
35. Song Y, Hu H, Feng M, Zhan H (2015) Carbon nanotubes with tailored density of electronic states for electrochemical applications. ACS Appl Mater Interfaces 7:25793–25803. doi:10.1021/acsami.5b07700
36. Arvand M, Ghodsi N (2014) Electrospun TiO_2 nanofiber / graphite oxide modified electrode for electrochemical detection of l-DOPA in human cerebrospinal fluid. Sensors Actuators B Chem 204:393–401. doi:10.1016/j.snb.2014.07.110